2007 IEEE International Conference on
Robotics and Automation
Roma, Italy, 10-14 April 2007

Whisker Sensor Design for Three Dimensional Position Measurement in Robotic Assisted Beating Heart Surgery

Ozkan Bebek, M. Cenk Cavusoglu
Department of Electrical Engineering and Computer Science
Case Western Reserve University, Cleveland, Ohio, 44106-7221, USA
E-mail: ozkan@case.edu, cavusoglu@case.edu

***Abstract*— In the robotic-assisted off-pump Coronary Artery Bypass Graft (CABG) surgery, surgeon performs the operation with intelligent robotic instruments controlled through teleoperation that replace conventional surgical tools. The robotic tools actively cancel the relative motion between the surgical instruments and the point of interest on the beating heart. Measuring the motion of the heart during this operation is an important part of this scheme. In this paper, a novel whisker sensor design to measure the heart motion in three dimensions (3-D) is presented. The proposed whisker sensor is a flexible contact sensor. Low stiffness of the sensor prevents damage on the tissue it contacts. This paper explains the design concept, and reports the simulation and measurement results of the prototype whisker position sensor.**

I. Introduction

Traditional off-pump Coronary Artery Bypass Graft (CABG) surgery is in a nascent stage and only applicable to limited cases. However, it is preferred over on-pump CABG surgery because of the significant complications resulting from the use of cardiopulmonary bypass machine, which include long term cognitive loss [1], and increased hospitalization time and cost [2]. Off-pump procedures represent only 15-20% of all CABG surgeries, at best [3]. Use of robotics technology will overcome limitations as it promises an alternative and superior way of performing off-pump CABG surgery on a beating heart with technical perfection equal to traditional on-pump procedures. This project aims to develop telerobotic tools to actively track and cancel the relative motion between the surgical instruments and the heart by Active Relative Motion Canceling (ARMC) algorithms, which will allow CABG surgeries to be performed on a stabilized view of the beating heart with the technical convenience of on-pump procedures.

In this paper, the design and implementation of a novel whisker sensor that is capable of measuring the position in three dimensions (3-D) are discussed. A whisker sensor can be used to detect the relative motion between the surgical instrument and the heart. These measurements are used in the tight control loop for active tracking of the heart.

Details about the system concept and related work in literature are presented in Section II. Design specifications of the sensor is provided in Section III. Section III-B describes the use of strain gauges for position measurement. In Section III-C, mechanics of the flexure beams are modeled. Final element analysis and experimental results of the proposed designs are given in Sections IV and V.

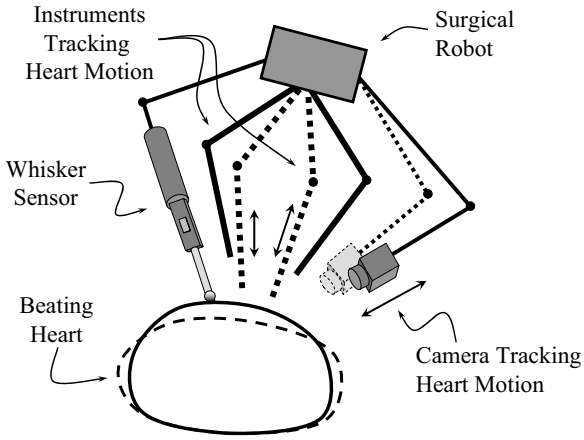

Fig. 1. System concept for Robotic Telesurgical System for Off-Pump CABG Surgery with Active Relative Motion Canceling (ARMC). Surgical instruments and camera mounted on a robot are actively tracing heart motion. Whisker sensor is in contact with heart, close to the point of interest.

II. System Concept and Use of Sensors

The robotic-assisted surgery concept replaces conventional surgical tools with robotic instruments which are under direct control of the surgeon through teleoperation. The surgeon views the surgical scene on a video display with images provided by a camera mounted on a robotic arm that follows the heart motion, showing a stabilized view. The robotic surgical instruments also track the heart motion, canceling the relative motion between the surgical site on the heart and the surgical instruments. As a result, the surgeon operates on the heart as if it were stationary, while the robotic system actively compensates for the relative motion of the heart. This is in contrast to traditional off-pump CABG surgery where the heart is passively constrained to dampen the beating motion. Since this method does not rely on passively constraining the heart, it would be possible to operate on the side and back surfaces of the heart as well as the front surface using millimeter scale robotic manipulators.

An important part of this robotic system is the development of sensing systems. These sensing components will track the heart motion, monitor biological signals, and provide force feedback to the surgeons. Multi sensor fusion with complementary and redundant sensors will be used for superior performance and safety.

Among the commercially available sensors, possible sen-

sor choices for the beating heart surgery are the sonomicrometric sensor, multi-camera vision sensor, force/torque sensing on the slave manipulator, inertial sensor, and laser proximity sensor.

The earlier studies in canceling beating motion with robotic assisted tools mainly used vision based and ultrasound based sensory systems to measure heart motion. In [4], Nakamura *et al.* performed experiments to track the heart motion with a 4-DOF robot using a vision system to measure heart motion. The tracking error due to the camera feedback system was relatively large (error in the order of few millimeters in the normal direction) to perform beating heart surgery. Thakral *et al.* used a laser range finder system to measure one-dimensional motion of a rat's heart [5]. Groeger *et al.* used a two-camera computer vision system to measure local motion of heart and performed analysis of measured trajectories [6], and Koransky *et al.* studied the stabilization of coronary artery motion afforded by passive cardiac stabilizers using 3-D digital sonomicrometry [7]. Ortmaier *et al.* [8] and Ginhoux *et al.* [9] also used camera systems to measure motion of the heart surface for their estimation algorithms. Cavusoglu *et al.* used a sonomicrometry system to collect heart motion data from an adult porcine [10], and they showed the feasibility of a robotic system performing off-pump CABG surgery.

Measurement of heart motion with high precision and high confidence is required for precise tracking performance. Also, redundant sensing systems are desirable for safety reasons.

Looking back at earlier research findings one can easily see that experimental results of vision sensors were not satisfactory for tracking in beating heart surgery. Vision systems potentially have problems with noise and occlusions. Also their resolution is restricted. Noise performance can be improved by using fluorescent markers, but the occlusion problem remains significant, which is an important setback, especially during surgical manipulations. Measurement resolution of a vision system depends on the camera quality and the distance to the point of interest. Vision sensors can provide high precision measurements in the tangential directions, but their precision is low in the normal direction.

Inertial sensors are not suitable for stand-alone use in position measurements, due to drift problems. Laser proximity sensors are limited to one dimensional measurement and can not provide any information about tangential motion of the heart surface.

A sensor that is in continuous contact with the tissue is necessary for satisfactory tracking. The contact sensors used in measuring the heart motion in literature are limited to ultrasonic sensors. Although sonomicrometric sensors are very accurate, they have issues resulting from a peculiar form of noise from ultrasound echoes.

The whisker sensor, that we introduced in this study, is a high sensitivity sensor which looks very much like its biological counterpart, long projecting hairs or bristles, equipped with micro strain gauges, coming out from the tip of the surgical manipulator and touching the heart surface. Sonomicrometric sensor has been the sensor of choice in the earlier studies of this research. The advantage of whisker sensor over the sonomicrometric and vision based sensors is that whisker sensor will directly give the relative motion of the heart with respect to the robotic manipulator, whereas the sonomicrometric and vision sensors give the motion of the heart with respect to the base sensors, and is more prone to error in calibration between the base sensors and the robotic manipulator coordinate frame. The whisker sensor will therefore be appropriate to use in a tight control loop for active tracking of the heart.

Sensors for different scopes were developed within the general whisker sensor description given above. Berkelman *et al.* [11] designed a miniature force sensor with strain gauges to measure forces in three dimensions at the tip of a microsurgical instrument. Two sets of crossed beams are used as the elastic elements of the force sensor. In [12], Scholz and Rahn used an actuated whisker sensor to determine the contacted object profiles for underwater vehicles. This whisker sensor predicted contact point based on the measured hub forces and torques with planar elastica model.

The rest of the paper focuses on the mechanical design of the proposed whisker sensor.

III. Whisker Sensor Design

The aim of this work is to create a miniature whisker sensor to measure the position of point of interest on the heart surface during the off-pump Coronary Artery Bypass Graft (CABG) surgery. Design limitations include the size constraint to make the tool usable in minimally invasive operations. In order to work in contact with heart tissue a sensor design that has low stiffness was aimed. The operation range of the sensor is adjusted to fit the heart motion, 12 mm peek to peek max displacement in one direction [10]. Also the resolution of the sensor should be high enough to track the beating heart using the control algorithm described in [13].

Two possible design options are considered. Both designs require a one axis contactless linear position sensing element (i.e., a Linear Variable Displacement Transducer (LVDT)) and a two axes flexure strain gauge position sensor.

In order to provide low stiffness, the position information in the normal direction is to be measured with the linear position sensor. The position in the lateral axes are to be measured with strain gauges attached to flexure beams. Similar geometrical designs are used in flexural joint mechanism designs [14]. Flexural joints are preferred because of the absence of friction and backlash. A drawback of the flexural elements is their limited deflection, which needs to be considered during the design.

The first design option is to place a cross shaped flexible structure to the back of the linear sensor and measure the lateral motion on the tip of the sensor by measuring the strain in the legs of the cross structure (Figure 2). A similar design was used by Berkelman in [11] to measure force/torque values of the sensor tip. One major difference is the higher stiffness of their design, which was intended

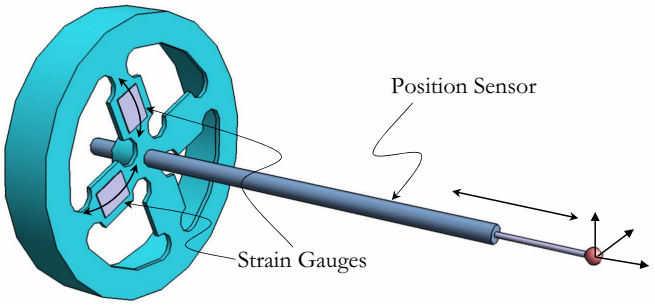

Fig. 2. Whisker Sensor Design 1: One linear position sensor and a × (cross) shaped flexible structure with strain gauges are used to measure the 3D position of the sensor tip.

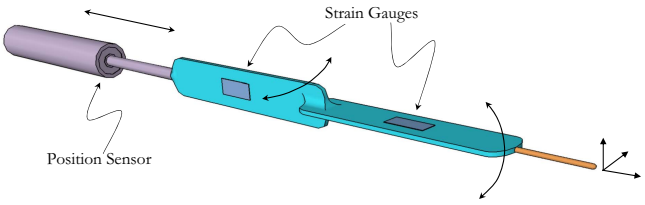

Fig. 3. Whisker Sensor Design 2: One linear position sensor and two flexure beams with strain gauges are used to measure the 3D position of the sensor tip.

for force sensing. The second design option is to fix two flexible cantilever beams orthogonally, so that the 2D lateral motion of the tip can be measured with strain gauge sensors placed on the beams by separating the motion into its two orthogonal components (Figure 3). As mentioned earlier, this kind of beam designs are used in flexure joint mechanisms [14].

These two designs are planned to be used with the system in a slightly different way due to their size differences. The design shown in Figure 2 can be manufactured in relatively smaller dimensions and it can be attached to the surgical tool to measure the displacement between heart and surgical tools. The other design shown in Figure 3 can be attached to the robotic manipulator base as shown in Figure 1, so that it can provide continuous contact even the surgical tools are not in close proximity to the heart, and measure the heart position.

Note that, due to the constraints of minimally invasive surgery, both of these designs are to be fitted inside a narrow cylindrical volume. The second design is relatively bigger in size with respect to the first design option since the linear transducer needs to support the flexure beams holding the strain sensors. This requires a structurally stronger and therefore a bigger linear sensor. In contrast, smaller linear sensors can be utilized in the first sensor design.

Our goal is to manufacture both sensor designs and check their feasibilities with the robotic system. In this paper, manufacturing details of the Whisker Sensor Design 2 will be explained, since the other design was still under construction when this paper was submitted.

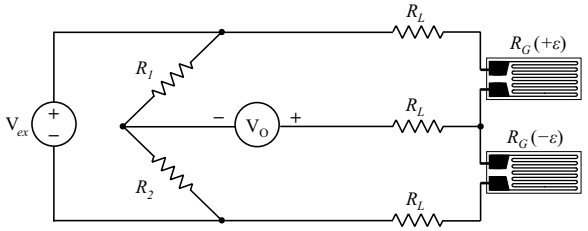

Fig. 4. Half Bridge Circuit: R_1 and R_2 are bridge completion resistors, R_L is the lead resistance and R_G is the nominal resistance of the strain gauges. V_{ex} is the excitation voltage and V_O is the measured output.

A. Equipment

As mentioned earlier, both designs require a one-axis contactless linear position sensing element, and a two-axes flexure beam strain gauge position sensing element. For the prototype built (Figure 3) the following equipment is used.

Linear Position Sensor: MicroStrain 24 mm stroke Subminiature Differential Variable Reluctance Transducer (DVRT−or half bridge LVDT) was used for the measuring the displacement in the normal direction. The sensor casing is 4.77 mm in diameter and sensor length is 132 mm at its maximum stroke. Resolution of the transducer is 5.7 μm with $\pm$ 1 μm repeatability. Its frequency response is 7 kHz.

Strain Gauges: Kyowa KFG-5-120-C1-11L1M2R type strain gauges with nominal resistance value, $R_G = 119.6 \pm 0.4\ \Omega$ and gauge factor, $GF = 2.11 \pm 0.4$ are used.

Signal Conditioning Equipment: National Instruments PCI-6023E 12-Bit Multifunction DAQ Board, SCXI-1121 4-Channel Isolation Amplifier and SCXI-1321 Offset-Null and Shunt-Calibration Terminal Block were used to acquire strain gauge and LVDT measurements.

SCXI-1121 module has 4 channel input with internal half-bridge completion. Module was configured for a voltage excitation, V_{ex}, of 3.333 V and a gain of 1000 for strain gauge measurements. At this gain, the input range of each channel is $\pm$1.7 mV, which can accommodate the $\pm$1.6 mV output of the bridge at its maximum stretch. The estimated resolution of the flexure beams are $\pm$3.2 μm and $\pm$5.8 μm. The resolution difference in the axes are due to the distance difference between the strain gauges and sensor tip.

B. Strain Calculations

In order to minimize the effect of temperature changes and increase the sensitivity of the circuit, half-bridge configurations are used to measure strains. Strain, ε, for the half-bridge configuration given in Figure 4 is [15]

$$\varepsilon = \frac{-2 \cdot (V_{O_{strnd}} - V_{O_{unstrnd}})}{GF \cdot V_{ex}} \cdot \left(1 + \frac{R_L}{R_G}\right), \quad (1)$$

where $V_{O_{strnd}}$ is the measured output when strained, $V_{O_{unstrnd}}$ is the initial, unstrained measurement and V_{ex} is the excitation voltage. $V_{O_{unstrnd}}$ is adjusted to 0 V by offset nulling beforehand. Offset nulling circuitry is used to rebalance the bridge and it also eliminates the effects of lead resistance. R_G is the nominal resistance value of strain gauge

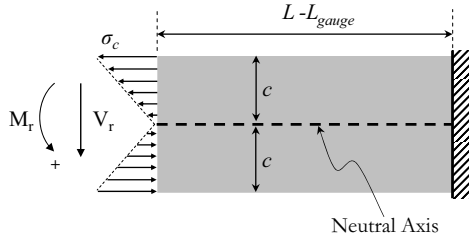

Fig. 5. Beam section forces and stresses at strain gauge position. σ_c is the normal stress acting on the surface of the transverse cross section. M_r is the resisting moment and V_r is the resiting shear force.

$(119.6 \pm 0.4\ \Omega)$, R_L is the lead resistance $(2.46\ \Omega/m)$ and GF is the gauge factor of strain gauge (2.11 ± 0.4). If R_G, R_L, GF and V_{ex} are substituted into (1), the final strain equation is

$$\varepsilon = -0.2905 \cdot V_{O_{strnd}}. \tag{2}$$

C. Mechanics of the Flexure Beams

Using the strain value found in the Section III-B, the position change of the tip of the sensor, (x_{tip}, y_{tip}), can be found using basic mechanics of materials [16]. The following assumptions are made to model the mechanics.

1) The gravitational effects on the beam are negligible.
2) The deflection of the beam is in the elastic range.
3) The square of the slope of the beam, $\left(\frac{dy}{dx}\right)^2$, is negligible compared to unity, where $y = f(x)$ is the elastic curve.
4) The beam deflection due to shearing stress is negligible (a plane section is assumed to remain plane).
5) Young's modulus, E, and the second moment of the cross sectional area, I, values remain constant for any interval along the beam.

Mechanics of the Cantilever Beam: The motion in the lateral plane of the flexure beams will cause two bending moments, M_x and M_y, in the sensor body. These can be calculated using the strain values, ε_x and ε_y, measured from the gauges attached on the cantilever beams. For linearly elastic action, the strain and stress relation can be defined by Hooke's law:

$$\sigma_x = E \cdot \varepsilon_x \tag{3}$$

where σ_x is the normal stress on a cross sectional plane and ε_x is the longitudinal strain. The normal stress will be maximum at the surface farthest from the neutral axis ($\sigma_{max} = \sigma_c$ at $y = c$, and c is half of the beam thickness, d). The normal stress at the surface, σ_c (Figure 5), can be found with strain measurement of the surface using Hooke's Law as given in (3).

The resisting moment is given as

$$M_r = -\frac{\sigma_c \cdot I}{c} = -\frac{\varepsilon_c \cdot E \cdot I}{c}\ . \tag{4}$$

The resisting moment acting at the point of strain gauge can be calculated using

$$M_r(L_{gauge}) = P \cdot L_{gauge}\ , \tag{5}$$

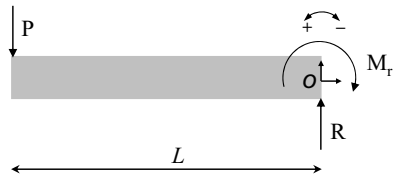

Fig. 6. Free body diagram of the cantilever beam. R is the reaction force at the supported end, M_r is the resisting moment and P is the bending force.

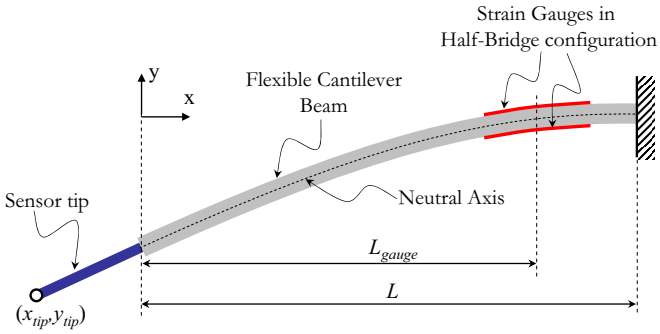

Fig. 7. Deflected Cantilever Beam

where P is the force acting on the unsupported end of the beam (Figure 6). Then, (4) can be rewritten as

$$P = -\frac{\varepsilon_c \cdot E \cdot I}{L_{gauge} \cdot c}\ . \tag{6}$$

During straight beam loading in an elastic action, the centroidal axis of the beam forms a curve defined as the elastic curve, $y = f(x)$. The differential equation for the elastic curve of the beam is

$$M(x) = E \cdot I \cdot \frac{d^2y}{dx^2} \tag{7}$$

where the moment, $M(x)$ is a function of x,

$$M(x) = P \cdot x \quad , \quad 0 \le x \le L\ . \tag{8}$$

If (7) is integrated twice, the elastic curve can be achieved. The beam's end point deflection, $y = 0$ at $x = L$, and end point slope, $\frac{dy}{dx} = 0$ at $x = L$, can be used as boundary conditions for the integration. Deflection curve and slope on the beam are given respectively as

$$y = -\frac{\varepsilon}{3 \cdot d \cdot L_{gauge}} \cdot (x^3 - 3 \cdot L^2 \cdot x + 2 \cdot L^3) \tag{9}$$

$$\frac{dy}{dx} = -\frac{\varepsilon}{d \cdot L_{gauge}} \cdot (x^2 - L^2)\ . \tag{10}$$

Then, the slope of the tangent line at the end point of the cantilever beam $(x = 0)$ is

$$\left.\frac{dy}{dx}\right|_{x=0} = \frac{\varepsilon \cdot L^2}{d \cdot L_{gauge}}\ . \tag{11}$$

It is assumed that the tool tip has high modulus of elasticity (rigid) and its deflection is negligible. Therefore

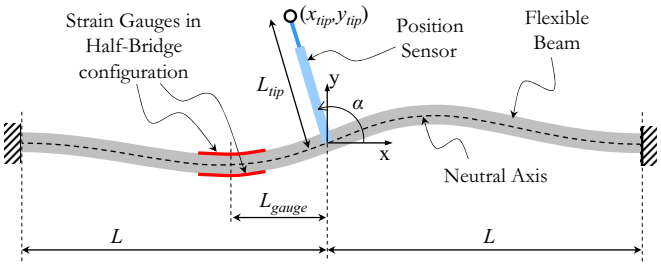

Fig. 8. Deflected Cross Beam Section

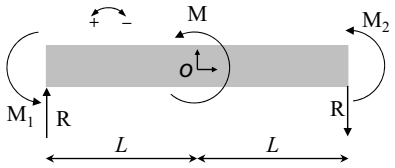

Fig. 9. Free body diagram of the cross beam section. R is the reaction force at the supported ends, M is the bending moment. M_1 and M_2 are the reaction moments at the supported ends.

its contact position can be calculated using the following line equation.

$$y_{tip} = \left(\frac{\varepsilon \cdot L^2}{3 \cdot d \cdot L_{gauge}} \right) \cdot (3 \cdot x_{tip} - 2 \cdot L) \tag{12}$$

Mechanics of the Cross Beam: Similar derivation methods can be used in this design. The motion in the lateral plane of the position sensor will cause two bending moments, M_x and M_y, on the cross flexure structure. These can be calculated using the strain values, ε_x and ε_y, and then the slope between the position sensor and the resting plane of the cross beam can be calculated.

From the free body diagram (Figure 9) a relation between reaction forces and bending moment can be found.

$$R = \frac{3\ M}{4\ L}\ , \tag{13}$$

where R is reaction force at the supporting ends. Then, the resisting moment, M_r, acting at the point of the strain gauge is

$$M_r(-L_{gauge}) = \frac{M\ (2L - 3L_{gauge})}{4L}\ . \tag{14}$$

Using (4) and (14), the bending moment can be calculated as

$$M = -\frac{8\ \varepsilon_c EIL}{d(2L - 3L_{gauge})}\ . \tag{15}$$

The moment distribution on the beam with respect to position can be derived as,

$$M(x) = \frac{M\ (3x + 2L)}{4L}\ , \qquad -L \le x \le 0^- \tag{16a}$$

$$M(x) = \frac{M\ (3x - 2L)}{4L}\ , \qquad 0^+ \le x \le L\ . \tag{16b}$$

The beam's end point deflections, $y = 0$ at $x = -L$ and $y = 0$ at $x = L$, and end point slopes, $\frac{dy}{dx} = 0$ at $x = -L$ and $\frac{dy}{dx} = 0$ at $x = L$, can be used as boundary conditions for the integration of the elastic curve equation given below.

$$E \cdot I \cdot \frac{d^2y}{dx^2} = \frac{3Mx}{4L} + \frac{M}{2}\ , \quad -L \le x \le 0^- \tag{17}$$

Deflection curve and slope of the beam respectively are

$$y = -\frac{\varepsilon\ x\ (x+L)^2}{d(2L - 3L_{gauge})} \cdot\ , \quad -L \le x \le 0^- \tag{18}$$

$$\frac{dy}{dx} = -\frac{\varepsilon\ (x+L)\ (3x+L)}{d(2L - 3L_{gauge})}\ , \quad -L \le x \le 0^-, \tag{19}$$

and the slope of the tangent line at the base of the position sensor ($x = 0$) is

$$\left.\frac{dy}{dx}\right|_{x=0} = -\frac{\varepsilon L^2}{d\ (2L - 3L_{gauge})}\ . \tag{20}$$

Therefore, slope of the position sensor is

$$\left.\frac{dy_p}{dx_p}\right|_{x_p=0} = \frac{d\ (2L - 3L_{gauge})}{\varepsilon L^2} = tan(\alpha)\ . \tag{21}$$

where

$$\left.\frac{dy_p}{dx_p}\right|_{x_p=0} \cdot \left.\frac{dy}{dx}\right|_{x=0} = -1\ . \tag{22}$$

Then, the angle of the position sensor with respect to the coordinate frame, α (Figure 8), is defined as

$$\alpha = \begin{cases} tan^{-1}\left(\frac{d\ (2L-3L_{gauge})}{\varepsilon L^2}\right), & \varepsilon > 0 \\ tan^{-1}\left(\frac{d\ (2L-3L_{gauge})}{\varepsilon L^2}\right) + \pi, & \varepsilon < 0 \\ \frac{\pi}{2}, & \varepsilon = 0 \end{cases}$$

It is assumed that linear position sensor has high modulus of elasticity (rigid) and its deflection is negligible. Therefore its contact position can be calculated using the following equations.

$$x_{tip} = L_{tip}\ cos(\alpha) \tag{23}$$

$$y_{tip} = L_{tip}\ sin(\alpha) \tag{24}$$

where L_{tip} is the overall length of the position sensor.

IV. Finite Element Simulation

Finite Element Model (FEM) analyses were done on the flexure beams to check the derived mathematical models (Figures 10, 11 and 12). Principle stress values (σ_{11}) were analyzed in the Finite Element Analysis (FEA) models. As the maximum stress on the surface of a deflected beam is equivalent to the principle stress value, corresponding strain values are calculated with principle stresses using Hooke's Law.

In this analysis, it was also confirmed that the affect of 2D lateral motion on the flexure beams can be separated into its two orthogonal components with the used flexure geometries (cross structured beams and orthogonally fixed cantilever beams). This enabled the use of strain gauges for measuring motion in 2D.

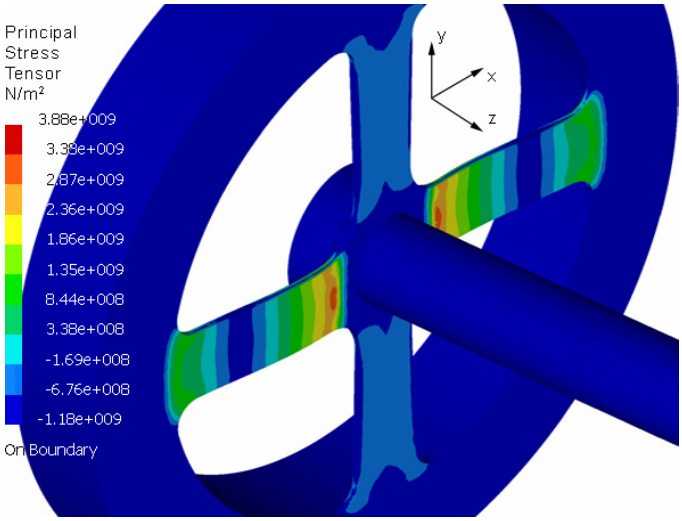

Fig. 10. FEA principal stress results of the cross flexure structure for a sensor tip displacement of 5 mm in the x-direction. Stress value at the strain gauge position is $1.51 \cdot 10^9$ N/m^2.

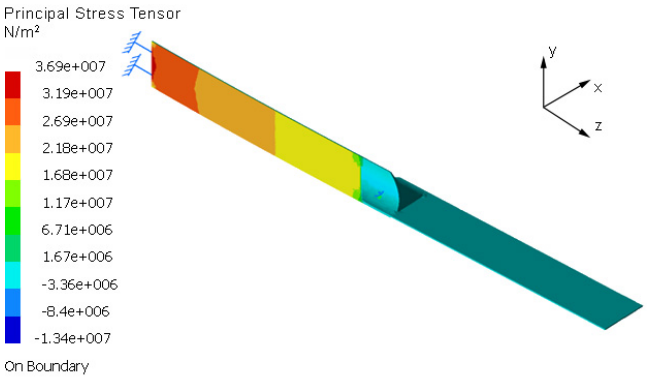

Fig. 11. FEA principal stress results of the flexure beam for a sensor tip displacement of 6 mm in the x-direction. Stress value at the strain gauge position is $2.60 \cdot 10^7$ N/m^2.

V. Experimental Results with the Prototype

The built prototype is shown in Figure 13. The flexure part of the prototype is tested in measuring predetermined distances. The validation of the measurements is done using a LVDT sensor. Simulation and experimental strain measurement results for constant sensor tip displacements are given in Table I. In simulations, the estimated strain values at the selected strain gauge positions on the beams are calculated. Actual strain gauge readings from the prototype sensor are reported for the experimental case.

As the mechanical structure of the beams gets complicated, the reported results starts to vary for the same element. For instance, reported results of the cantilever beam that measured the motion in y-direction are similar. This is mainly because of the geometrical simplicity of that element. Also, FEM results are affected by the deflection of sensor elements other than flexures (i.e., flexure joint elements, position sensors).

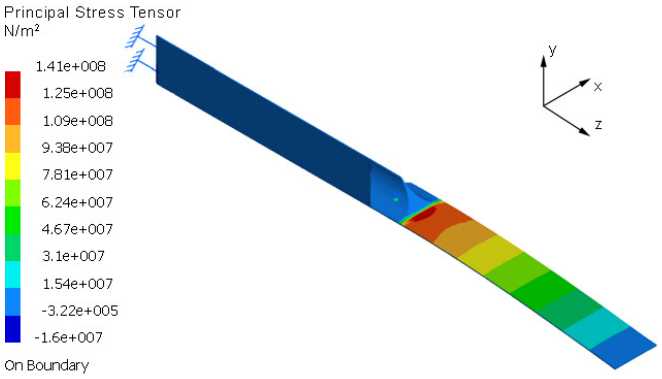

Fig. 12. FEA principal stress FEA results of the flexure beam for a sensor tip displacement of -6 mm in the y-direction. Stress value at the strain gauge position is $8.84 \cdot 10^7$ N/m^2.

TABLE I

Simulation and Experimental Strain Measurement Results for a Constant Sensor Tip Displacement: *In simulations, the estimated strain values at the selected strain gauge positions are calculated. Actual strain gauge readings from the prototype sensor are reported for the experiment case.*

Strain Measurements	Design 1	Design 2	
Tip Displacement	5 mm	6 mm	
Bending Flexure Element	X or Y	X	Y
Unit	m/m		
Mathematical Model	$8.59\ 10^{-3}$	$2.38\ 10^{-4}$	$4.50\ 10^{-4}$
FEM Analysis	$7.80\ 10^{-3}$	$1.39\ 10^{-4}$	$4.58\ 10^{-4}$
Experimental Value	–	$1.71\ 10^{-4}$	$4.49\ 10^{-4}$

Conclusions

In this paper, a novel position sensor to measure beating heart position in an minimally invasive beating heart surgery is presented. The manufactured prototype showed that use of proposed whisker sensors are promising. Next step in this work will be to manufacture a prototype for Design 1. Also, flexure beams dimensions in Design 2 will be optimized for more uniform resolution in every direction.

Acknowledgment

This work was supported in part by the National Science Foundation under grants CISE IIS-0222743, EIA-0329811, and CNS-0423253, and US DoC under grant TOP-39-60-04003.

References

[1] M. F. Newman, J. L. Kirchner, B. Phillips-Bute, V. Gaver, H. Grocott, R. H. Jones, *et al.*, "Longitudinal assessment of neurocognitive function after coronary-artery bypass surgery," *New England Journal of Medicine*, vol. 344, no. 6, pp. 395–402, February 2001.

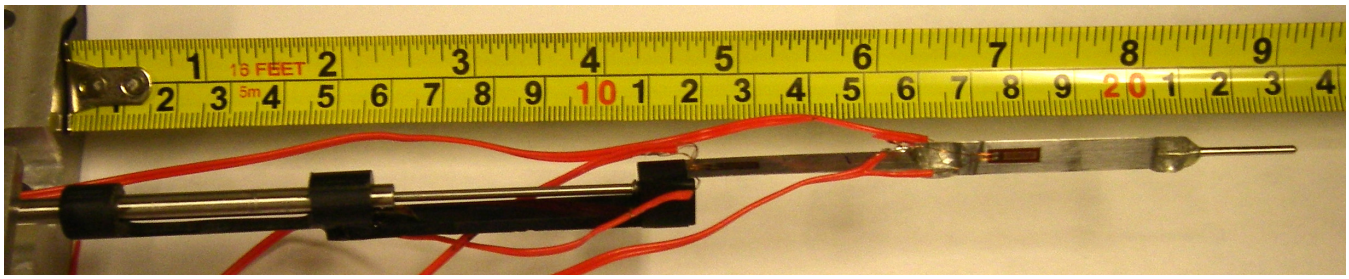

Fig. 13. Prototype of the Whisker Sensor Design 2: Overall length of the sensor when the linear stage is all the way in is 21.3 cm, and 23.9 cm when the linear stage is all the way out (as shown here). The largest diameter of the prototype is 12.5 mm.

[2] J. D. Puskas, C. E. Wright, R. S. Ronson, W. M. Brown, J. P. Gott, and R. A. Guyton, "Off-pump multi-vessel coronary bypass via sternotomy is safe and effective," *Annals of Thoracic Surgery*, vol. 66, no. 3, pp. 1068–1072, September 1998.

[3] M. B. Ratcliffe, *Personal Communication*, MD, Chief of Surgery, San Francisco VA Medical Center, Professor in Residence.

[4] Y. Nakamura, K. Kishi, and H. Kawakami, "Heartbeat synchronization for robotic cardiac surgery," in *Proc. of IEEE International Conference on Robotics and Automation (ICRA)*, vol. 2, 2001, pp. 2014–2019.

[5] A. Thakral, J. Wallace, D. Tomlin, *et al.*, "Surgical motion adaptive robotic technology (S.M.A.R.T.): Taking the motion out of physiological motion," in *Proc. of 4th International Conference on Medical Image Computing and Computer-Assisted Intervention (MICCAI)*, October 2001, pp. 317–325.

[6] M. Groeger, T. Ortmaier, W. Sepp, and G. Hirzinger, "Tracking local motion on the beating heart," in *Proc. of the SPIE Medical Imaging Conference*, vol. 4681 of SPIE, San Diego, CA, USA, February 2002, pp. 233–241.

[7] M. L. Koransky, M. L. Tavana, A. Yamaguchi, and R. Robbins, "Quantification of mechanical stabilization for the performance of offpump coronary artery surgery," in *Proc. of the Meeting of the International Society for Minimally Invasive Cardiac Surgery (ISMICS)*, 2001, (Abstract).

[8] T. Ortmaier, M. Groeger, D. H. Boehm, V. Falk, and G. Hirzinger, "Motion estimation in beating heart surgery," *IEEE Trans. Biomed. Eng.*, vol. 52, pp. 1729–1740, October 2005.

[9] R. Ginhoux, J. A. Gangloff, M. F. DeMathelin, L. Soler, J. Leroy, M. M. A. Sanchez, and J. Marescaux, "Active filtering of physiological motion in robotized surgery using predictive control," *IEEE Trans. Robotics*, vol. 21, no. 1, pp. 67–79, February 2005.

[10] M. C. Cavusoglu, J. Rotella, W. S. Newman, S. Choi, J. Ustin, and S. S. Sastry, "Control algorithms for active relative motion cancelling for robotic assisted off-pump coronary artery bypass graft surgery," in *Proc. of the 12th International Conference on Advanced Robotics (ICAR)*, Seattle, WA, USA, July 2005, pp. 431–436.

[11] P. J. Berkelman, L. L. Whitcomb, R. H. Taylor, and P. Jensen, "A miniature microsurgical instrument tip force sensor for enhanced force feedback during robot-assisted manipulation," *IEEE Transactions on Robotics and Automation*, vol. 19, no. 5, pp. 917–922, October 2003.

[12] G. R. Sholz and C. D. Rahn, "Profile sensing with an actuated whisker," *IEEE Transactions on Robotics and Automation*, vol. 20, no. 1, pp. 124–127, February 2004.

[13] O. Bebek and M. C. Cavusoglu, "Predictive control algorithms using biological signals for active relative motion canceling in robotic assisted heart surgery," in *Proc. of the International Conference on Robotics and Automation (ICRA)*, Orlando, FL, USA, May 2006, pp. 237–244.

[14] M. P. Koster, "Flexural joints in mechanisms," in *Proceedings of the ASME Dynamic Systems and Control Division*, 2000, pp. 855–859.

[15] "Strain gauge measurement - a tutorial," National Instruments, Tech. Rep. 078, August 1998.

[16] W. F. Riley, L. D. Sturges, and D. H. Morris, *Mechanics of Materials*, 5th ed. New York, USA: John Wiley & Sons Inc., 1999.